PARAMETERS FOR STUDY 2
Version 2

R.B. Palmer[1], S. Berg[1], R. Fernow[1], Y. Fukui[2], J. Gallardo[1], C. Kim[3], E. Kim[3], H. Kirk[1], J. Miller[4], N. Mokhov[5], G. Penn[3], R. Weggel[1], J. Wurtele[3]

[1]BNL, Upton, NY 11973, USA

[2]UCLA, Los Angeles, CA 90024, USA

[3]LBNL, Berkeley, CA 94720, USA

[4]NHNFL, Berkeley, FL 32310, USA

[5]FNAL, Batavia, IL 60510, USA

March 9, 2001

Abstract

The parameters are given for the front end of a Neutrino Factory. No rf is employed near the target and relatively little polarization (22 %) is achieved, but the efficiency of producing muons is good (≈ 0.17 μ/p with 24 GeV proton bunches with 3 ns rms length). Per MW of proton power, this is 6.2 $\times$ the performance of Feasibility Study I [1].

The high efficiency is achieved by:

1. using a liquid mercury target;
2. using three induction linacs and long drifts to achieve near non-distorting phase rotation into a longer bunch train and less momentum spread; and
3. tapering the focus strength in the cooling system so that the angular spread of the muons being cooled is maintained at a near constant value.

1 Contents

2 List of Figures

3 List of Tables

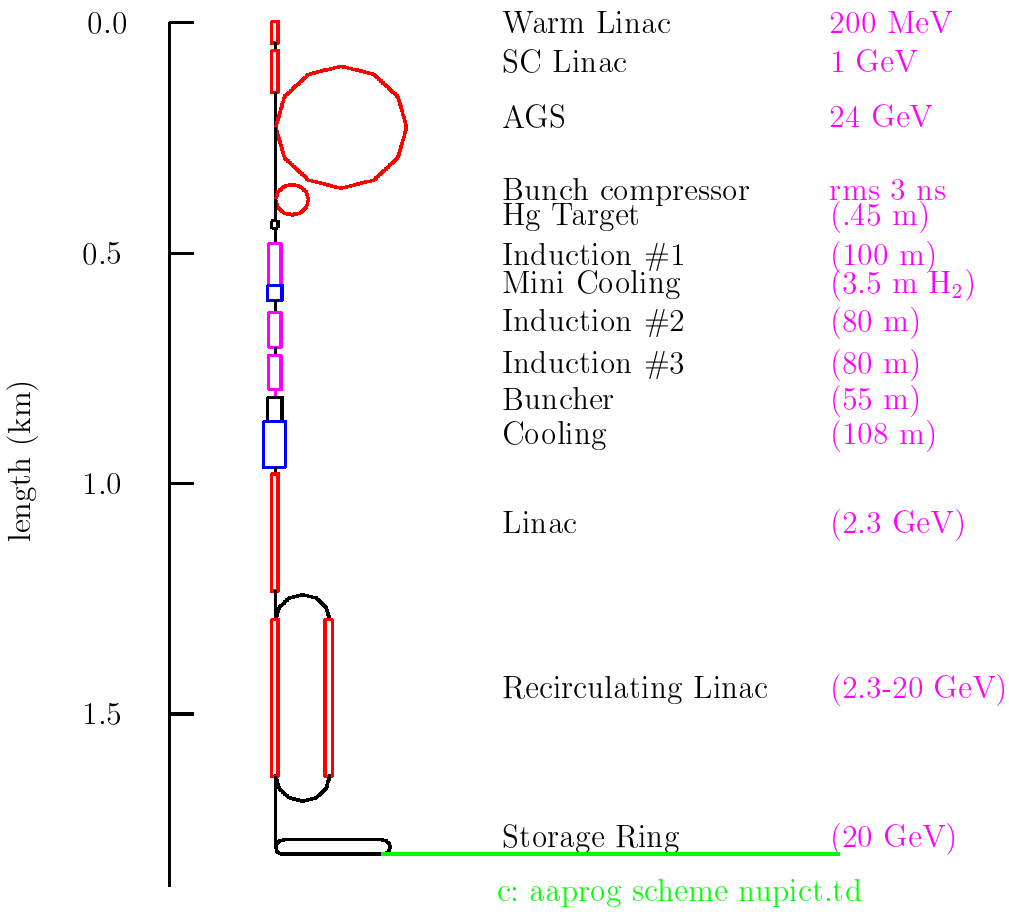

Figure 1: Schematic of the Neutrino Factory Facility

4 INTRODUCTION

This note gives specifications and a summary of simulation results for Feasibility Study II Neutrino Factory. The scheme is illustrated in Fig. 1

The lengths of the main components are listed in the Tb. 1

5 SPECIFICATIONS

5.1 Proton driver

The proton driver secifications are given in Tb 2. Finite time between bunches is required for a number of reasons:

Table 1: Length of the main components of a Neutrino Factory

Component	Length m	Total m
target	0.45	0.45
taper	17.6	17.6
drift	18	35.6
Induction 1	100	135.6
Drift	5	140.6
Mini-Cool	10	150.6
Drift	35	185.6
Induction 2	80	265.6
Drift	20	285.6
Induction 3	80	365.6
Match to Super FOFO	17.5	383.1
Buncher	$20 \times 2.75 = 55$	438.1
cooling part 1	$16 \times 2.75 = 44$	482.1
match	4.4	486.5
cooling part 2	$36 \times 1.65 = 59.4$	545.9
Linac	275	
RLA arcs	270	
RLA linacs	2×366	
Storage ring arcs	2×53	
Storage ring straights	2×216	

Table 2: Parameters of the proton driver

Energy	24	GeV
protons per bunch	$\approx 1.7 \ \ 10^{13}$	
bunches per fill	6	
time between extracted bunches	20	ms
repetition rate	2.5	Hz
rms bunch length	≤ 3	ns
beam power	≥ 1	MW
normalized emittance (95%)	mm mrad	100
normalized emittance (rms)	mm mrad	17

- To allow time to refill the RF cavities in the accelerating systems and avoid excessive beam loading;

- To avoid the need for multi pulsing of the induction linacs; and

- to allow the liquid target to be re-established after its assumed dispersal by the previous bunch. The specified spacing of 20 ms is based on the assumption that the jet has a velocity of 30 m/sec and that the jet, including that part between the nozzle and start of interaction with the beam, is fully dispersed.

The possibility of an average power greater than 1 MW, up to 4 MW is considered in appendix ***.

Lengths or circumferences of the major components are given in tb. 3

Table 3: Lengths or circumferences of the major components

	length m	ΔE GeV	f MHz
Conventional linac	150	0.2	200
SC linac	55	.2-.7	??
SC linac	88	.7-1.5	??
AGS synchrotron	807	1.5-24	??
Fixed field buncher ring	202	24	??

5.2 Target

Geometry A single proton bunch will heat the target to a temperature to several hundred degrees C and generate substantial shock pressures. A low Z target, as proposed in Study 1[1], is expected to survive these shocks for a significant time with a 1 MW beam, but is predicted to have a pion production almost a factor of 2 lower than with highj z targets such as inconel, or mercury. It would also expected to get too hot with a 4 MW beam: a possible upgrade. A liquid mercury jet target, on the other hand, is expected to be dirupted by the heating from the beam, but such disruption is not expected to have significant adverse consequences, even at 4 MW, and is thus selected as the baseline for this study. If there were unexpected problems with mercury, other liquids such as a molten lead/tin eutectic, or other alloy, could be used. A moving band of inconel, as discussed in appendix *** would also be an alternative. A graphite target (as used in study I) could also be considered as a backup, but would reduce the neutrino intensity by a factor of 1.9 (see [1] section 3.5).

In this Study, the beam with rms radius σ_r, at an angle θ_p, intersects the mercury jet of radius r_o and angle θ_{Hg} at an angle $\theta_{crossing}$. The forward velocity of the jet is v_o. The intervals between pulses is t, and it will be assumed here that after a pulse, all the mercury outside of the nozzle is dispersed. The nozzle is at z_{nozzle} with respect to the intersection of the beam and jet center lines. These parameters are given in tb. 4.

The geometry is shown if Fig. 2. The intersection of the beam and jet is set at 45 cm from the nozzle. The distribution of the resulting interactions as a function of z is shown at the top of the figure. It is seen that this distribution starts about 15 cm from the nozzle. At the time of a subsequent bunch, the newly established jet will extend a distance $\Delta z = v_o\ t = 0.6$ m

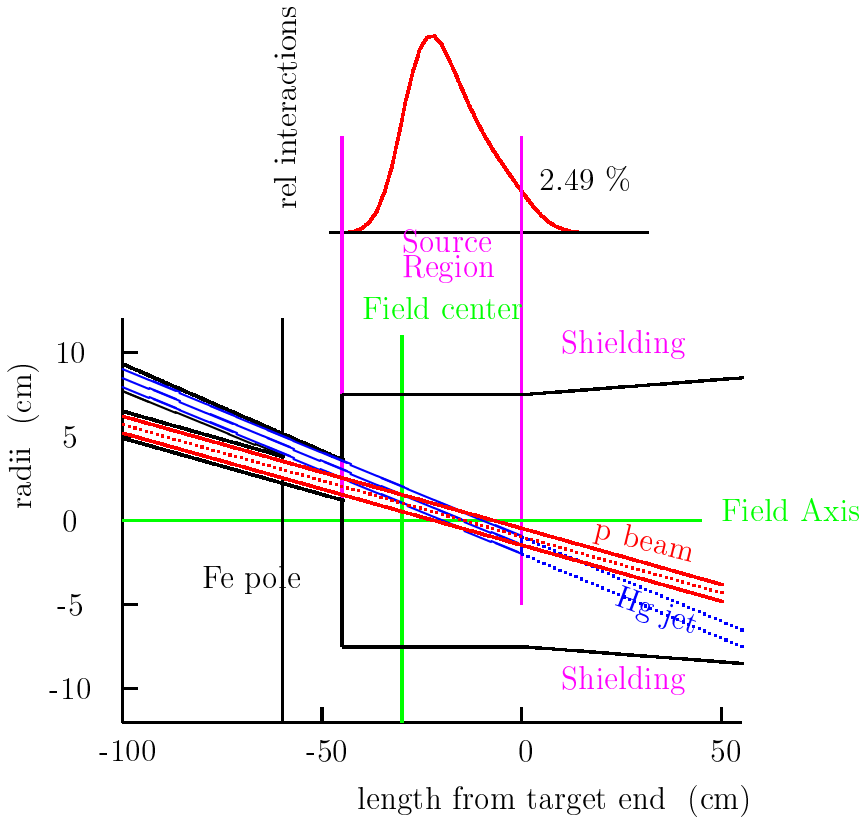

Figure 2: Top: Distribution of interactions as function of z. Bottom: Layout of the target area.

Table 4: Proton beam and mercury jet geometric parameters.

beam σ_r	1.5	mm
beam angle to magnet axis θ_p	67	mrad
jet material	mercury	
velocity v_o	30	m/sec
jet radius r_o	5	mm
jet angle to magnet axis θ_{Hg}	100	mrad
crossing angle $\theta_{crossing}$	33	mrad
t between bunches	20	ms

from the nozzle. It is seen that only 2.5 % of the interactions would occur after this location, so the disposition of the disturbed jet beyond this point can have little effect on production.

The only distance over which the jet must propagate without serious magnetic disruption is from the nozzle to a point 0.6 m downstream, defined as $z = 0$ in accordin ate system used here. In order to minimize the field non uniformity over this length, the magnetic center (approximate point of maximum B_z is placed at the center of this length. i.e. the magnetic center is set at a location of $z_o = -30$ cm in this coordinate system. The intersection of the

jet and beam is then at $z_{intersection} = \ -15$ cm, and the nozzle is at $z_{nozzle} = -60$ cm.

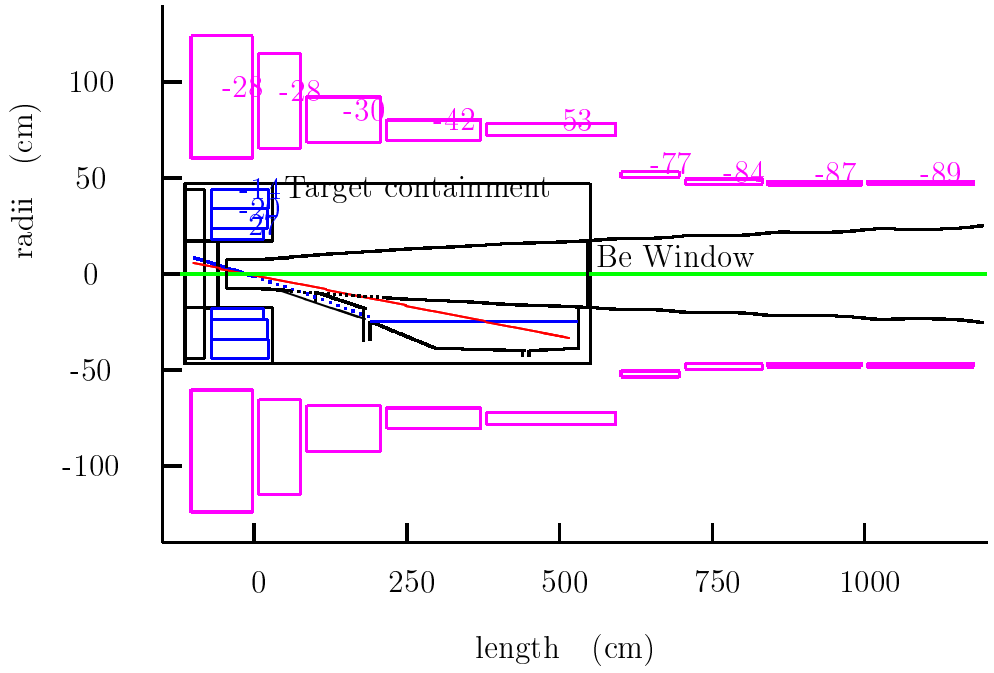

Figure 3: Target, Capture Solenoids and mercury containment

Capture and matching Solenoids The target is located in a 20 T solenoid to contain transverse momenta of outcoming pions up to 225 MeV/c, a large fraction of all such pions. The central region of high field is designed to have an rms width of 80 cm, in order to limit magnetic disruption of the jet. The solenoid is a hybrid, with copper (insert) and superconducting (outsert). It is similar to that discussed[1] in Feasibility Study I. However, it is proposed here to use hollow copper conductor for the insert, rather than a Bitter style magnet in Study I. The choice is aimed at achieving a magnet life over 40 years (compared with *** months in Study 1), and avoiding possible corosion problems with the highly irradiated wet insulation in a Bitter magnet. It is understood that the initial cost will be higher.

After the 20 T magnet, coils are designed to taper the axial field down slowly to 1.25 T over a distance of approximately 18 m. The form of the tapered field is approximately:

$$B(z) \ \approx \ \frac{20}{1 \ + k \ z}$$

Dimensions of coils and iron pole are given in the following table 5

The coils are shown in Fig. 3, and the axial field profile, over two scales of z, are shown in Fig. 5.2. The dotted line in the second plot is for a Gaussian with $\sigma_z = .8$ m.

Table 5: Proton beam and mercury jet geometric parameters.

len1 m	gap m	dl m	rad m	dr m	I/A A/mm^2	n I A	n I l A m
Fe							
0.980	0.980	0.108	0.000	0.313	0.00	0.00	0.00
1.088	-.000	0.312	0.000	0.168	0.00	0.00	0.00
Cu coils							
1.288	-.112	0.749	0.178	0.054	-24.37	0.98	1.26
1.288	-.749	0.877	0.231	0.122	-19.07	2.04	3.74
1.288	-.877	1.073	0.353	0.137	-14.87	2.18	5.78
SC coils							
0.747	-1.614	1.781	0.636	0.642	-23.39	26.77	160.95
2.628	0.100	0.729	0.686	0.325	-25.48	6.04	32.23
3.457	0.100	0.999	0.776	0.212	-29.73	6.29	34.86
4.556	0.100	1.550	0.776	0.107	-38.26	6.36	33.15
6.206	0.100	1.859	0.776	0.066	-49.39	6.02	30.59
8.000	-.065	0.103	0.416	0.051	-68.32	0.36	1.00
8.275	0.172	2.728	0.422	0.029	-69.27	5.42	14.88
11.053	0.050	1.749	0.422	0.023	-75.62	3.00	8.18
12.852	0.050	1.750	0.422	0.019	-77.37	2.61	7.09
14.652	0.050	1.749	0.422	0.017	-78.78	2.30	6.22
16.451	0.050	1.750	0.422	0.015	-79.90	2.07	5.59
18.251	0.050	2.366	0.422	0.013	-80.85	2.53	6.80

Table 6: Relevant properties of Hg.

B_o	20	T
σ'_z	.8	m
κ	10^6	Ω m
ρ	13.5 10^4	kg/m^3
T_{surface}	.456	N/m

Magnetic disruption of jet Assuming Gaussian distribution of B'_z vs z', with a maximum value of B_o, and jet conductivity κ, density ρ, and surface tension $T_{surface}$, as given in Tb. 6, perturbation calculations [?] show that over the extent of the new jet (from - .6 to 0 m):

- The maximum axial field deviations are +/− 1.1 T = 5%
- The axial pressure difference has a minimum of - 0.25 atmospheres. Thus if the jet is operating in a gas (He or Argon) at a pressure greater than or equal to .25 atmosphere,

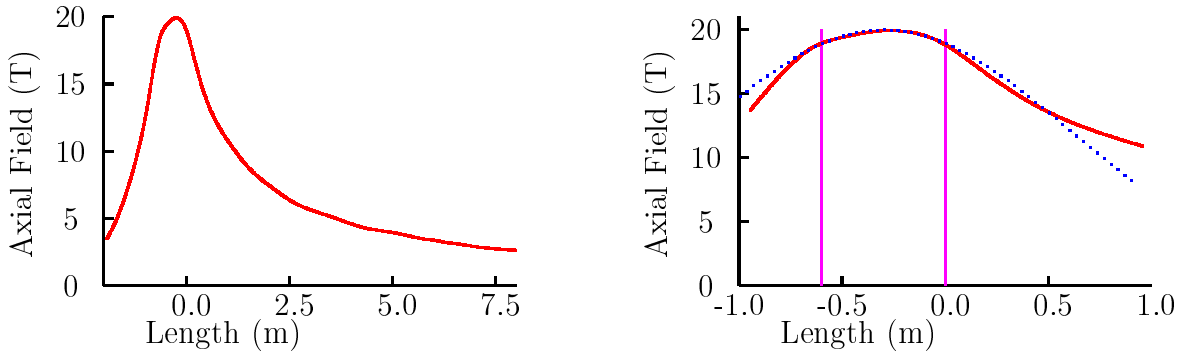

Figure 4: Red lines: axial capture magnetic field vs. length, with two scales. Blue dots give a Gaussian fit to the field in the jet region with $\sigma_z = .8$ m.

then the negative pressures will be avoided, and there will be no tendency to cavitate prior to the arrival of the beam.

- The maximum average deceleration of the jet is very small compared to the average jet velocity: 0.06/30≈0.2%.
- The maximum decelerations (from shear forces) are also small compared to the average jet velocity: 0.4/30≈1.3%.
- The deflections of the jet are very small: 5 μm.
- The jet distortions (Δ width / ave width) are approximately 0.4% without surface tension, and less than 0.2% with surface tension.

These disruptions are all relatively small, and should cause no problems. Beyond the target region (z=0 to 1.5 m), the effects are larger, but still not sufficient to break up the jet. The maximum shear is about 5 m/sec, and the distortion 20 %. But these numbers are probably meaningless, since the jet will have been disrupted by the beam.

Shielding and Mercury Containment Fig 3 also shows the concepts for mercury containment and the mercury pool beam dump. Fig 5 gives some more details. In order to remove this containment, the hollow conductor coils must also removed, either first, or at the same time. Note that the mercury jet, or what remains of it, falls under gravity, and thus further separates from the beam axis. A system of grids or baffles is introduced to slow the mercury spray before it joins the beam dump mercury pool. Note that the outflow pipe must be quite large (it is drawn as 10 cm diameter) in order to take the considerable rate of filling from the jet. The drain would only be opened when emptying the contaiment for its removal.

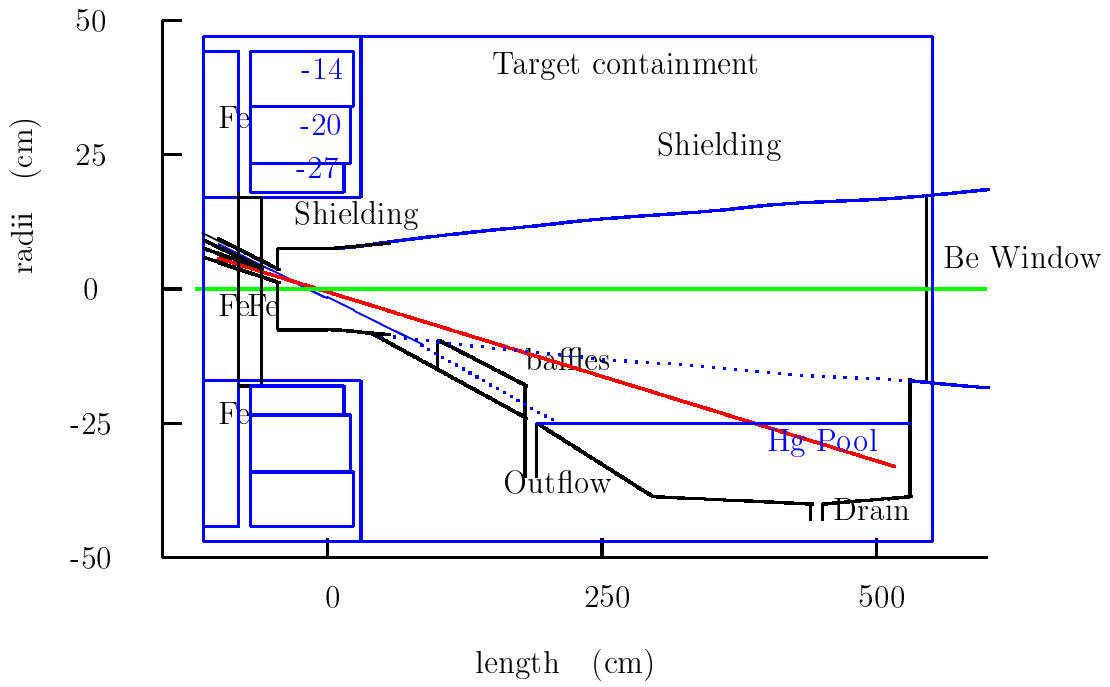

Figure 5: Beam dump, shielding and mercury containment detail

Figure 6 shows the radiation per 2 10^7 secs in the worst lengthwise section of the capture system. Figure 7 shows the radiation per 2 10^7 secs in the worst transverse section (at z=10 cm). Table 7 gives the maximum doses per year and expected lifetime at the worst location of various components. Note that Figs. 6 and 7 gave the radiation a 2 10^7 sec year, but Table 7 gives the doses per 1 10^7 sec year, consistent with this papers conventions.

Table 7: Radiation doses and lifetimes of some components ***needs updating

Component	radius cm	Dose/yr Grays/10^7 sec	Max allowed Dose Grays	1MW Life years	4 MW life years
Inner Shielding (SS)	7.5	2.5 10^{10}	10^{12} *	40	10
Hg Containment (SS)	18	5 10^8	10^{11}	200	50
Hollow Conductor (SS)	18	5 10^8	10^{11}	200	50
Superconducting Coil	65	1 10^6 **	10^8	100	25

* Assuming that stainless steel can withstand this dose so long as it is not stressed. Cu is claimed to take it, but is not compatible with Hg. If SS will not, then we should try and find something that would. It is assumed that this shielding would be cooled by mercury.

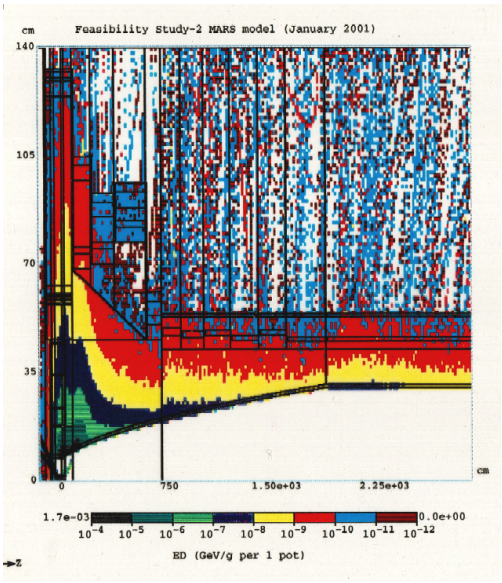

Figure 6: Radiation in worst section of capture system *** Needs update from Nikolai

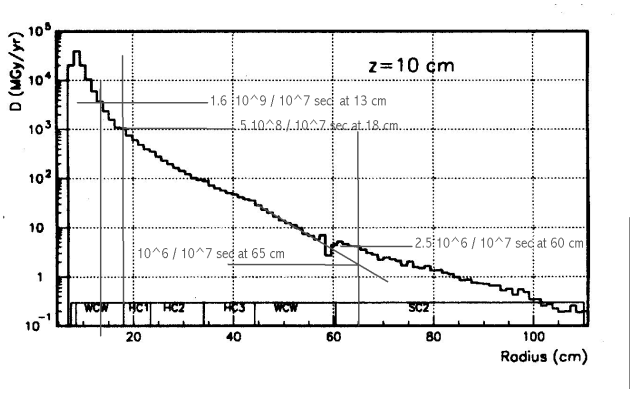

Figure 7: Radiation vs. r at worst z *** Needs updadate from Mokhov

5.3 Beam Transport and field reversal

Beam Transport After the 20 T capture solenoid and tapered field down to 1.25 T, the beam is transported through drift sections, the phase rotation linacs, and the mini-cooling hydrogen absorbers, in a transport channel consisting of solenoid coils with a 50 cm periodicity. The coil radii are larger at the beginning to allow space for shielding.

Field Reversal Between the two hydrogen absorbers, there is a 10 m long chromatically matched field reversal. This reversal is needed for two reasons:

Table 8: Phase rotation channel

length	18-48	48-148	148-368	m
bore radius	30	30	30	cm
coil IR	38	33	32.5	cm
coil thickness	.8-1	.8-1	.8-1	cm
axial field	1.25	1.25	1.25	T
coil periodicity	50	50	50	cm
coil lengths	36	36	36	cm

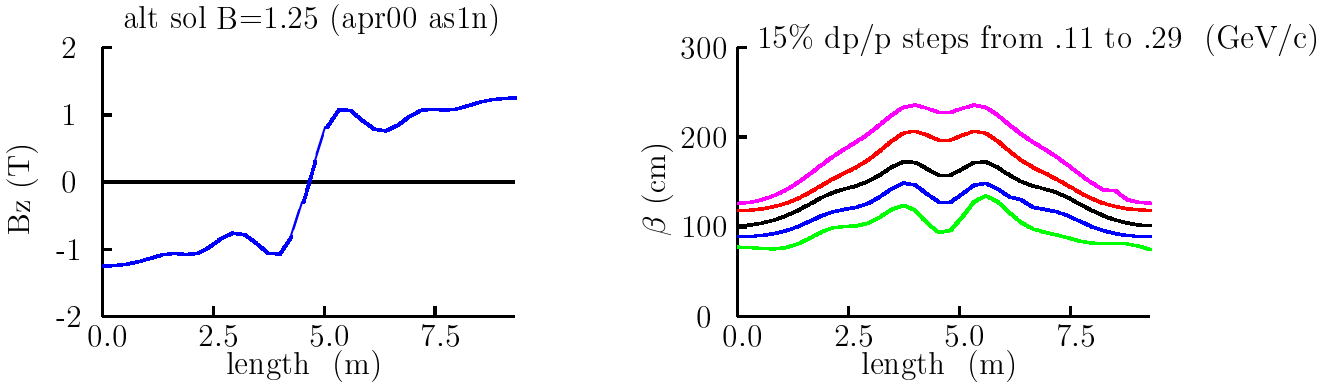

Figure 8: Left: Field reversal: B_z on axis; rigth: β function as a function of z for momentum between $0.11 - 0.29$ GeV/c.

- between two halves of the absorber, it is needed to avoid generating finite canonical angular momentum from the reduction of angular momentum in the absorbers; and
- at some point along the phase rotation a field reversal is needed to avoid generating a correlation between the canonical angular momentum of individual tracks and their energy after correction by the induction units.

By serendipity, a single flip appears to meet both requirements.

The field reversal was designed to match β's from start to end, over a momentum interval of 200 +/− 90 MeV. The axial fields through this reversal are given table 9, and plotted in the Fig. ??, together with the β's obtained for a set of different momentum.

5.4 Phase Rotation

Introduction Induction linacs combined with drifts and hydrogen absorbers are used to 'phase rotate' the beam. After a drift, low energy particles which fall back in the bunch are accelerated, while the high energy particles which remain in the front of the bunch are decelerated. As a result, a distribution that has an initially large energy spread, but short

Table 9: Longitudinal field on axis for the field reversal matching.

length m	Field T	continued	
.000	-1.25	6.1043	.78483
.2655	-1.2446	6.3697	.76088
.5309	-1.2242	6.6351	.84302
.7963	-1.1874	6.9005	.97396
1.0617	-1.1357	7.1659	1.0659
1.3271	-1.0852	7.4313	1.0802
1.5925	-1.0664	7.6967	1.0664
1.8579	-1.0801	7.6967	1.0664
2.1233	-1.0661	7.6967	1.0664
2.3887	-.97434	7.6967	1.0664
2.6541	-.84339	7.6967	1.0664
2.9195	-.76098	7.6967	1.0664
3.1849	-.78458	7.6967	1.0664
3.4503	-.9125	7.6967	1.0664
3.7157	-1.0631	7.6967	1.0664
3.9811	-1.0747	7.6967	1.0664
4.2465	-.81469	7.9621	1.0851
4.5119	-.30422	8.2275	1.1355
4.7773	.30242	8.4929	1.1873
5.0427	.81346	8.7583	1.2241
5.3081	1.0744	9.0237	1.2445
5.5735	1.0635	9.2891	1.251
5.8389	.913	10.0	1.25

time spread, is rotated into a bunch with small energy spread but long time spread. If the process is done with a single drift and single induction linac, then relativistic effects cause a distortion of the rotated bunch such that the initially high energy particles end with a larger energy spread than the initially low energy ones. The use at least two induction linacs, with a drift between them, allows this distortion to be greatly reduced[?].

It is natural for both these induction linacs to be bipolar, with initial decelleration and later acceleration. For technical reasons, such bipolar voltage pulses have been avoided in the baseline design. In the case of the first linac, a hydrogen absorber imediatgely after it to reduce the beam energy, allowing the first linac to be unipolar. This absorber also reduces the emittance, and is thus refered to as a "mini-cooler'. The absorber is in two parts with the field reversal between them to avoid the generation of angular momentum.

To avoid a bipolar second linac, it has been repalced with two linacs: the first unipolar decellerating, the second unipolar acceleration (A slightly less conventional bipolar second linac solution is discussed in section ??).

Induction Linacs A first linac is introduced close to the target and forms the time energy distribution to give non-distorting phase rotation later. The combination of the second and third induction linacs remove the energy dependence on time. The parameters of the linacs are given i Tb. 11, and the shape of the accelerating pulse is given in Fig. 9.

Table 10: Induction Linacs

		1	2	3
length	m	100	80	80
inner radius	cm	30	30	30
Solenoid field	T	1.25	1.25	1.25
maximum gradient	MV/m	1.55	1.45	1.0
pulse length	nsec	190	100	360

Table 11: Length of the pulse and gradient of the 3 induction linacs

Ind	1	Ind	2	Ind	3
t	G	t	G	t	G
nsec	MV/m	nsec	MV/m	nsec	MV/m
5	0.0	-34	0.0	-15	0.0
15	29.1	-24	-145.0	10	7.5
30	65.9	-14	-145.0	35	32.5
50	93.8	-4	-118.8	60	48.8
90	123.3	6	-70.0	85	63.8
130	139.4	16	-53.1	110	70.0
170	155.0	26	-37.5	135	78.1
190	135.0	36	-28.1	160	82.5
200	50.0	46	-21.3	185	90.0
220	0.0	56	-15.6	210	96.3
		66	-10.6	235	99.4
		76	-6.3	260	100.0
		86	-3.1	285	100.0
		96	-1.3	310	100.0
		106	0.0	335	100.0
				360	62.5
				385	0.0

Mini-cooling Hydrogen absorbers Between the first and second induction linacs, hydrogen is introduced to lower the energies and reduce the transverse emittance. The hydrogen is divided into two parts (1.75 m long each) with a chromatically matched field reversal between them.

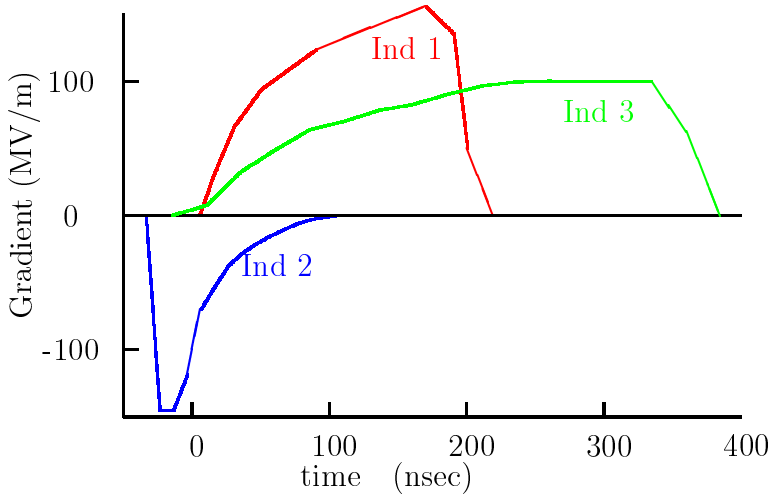

Figure 9: Induction Linac: Gradient pulse shapes in time

At the front of the first hydrogen absorber there is a thick cooled room temperature Be absorber to take the energy from low energy particles in the beam pipe and avoid excessive heating of the hydrogen.

The parameters are given in Tb. 12. The Energy deposited in the initial window and in the hydrogen, is significant and is cooled by ***.

Table 12: Mini-cooling parameters ***

radius	30	cm
Be window thickness	??	cm
Energy deposited in Be	??	kW
first hydrogen length	1.75??	m
Energy deposited in first H2	??	kW
second hydrogen length	1.75	m
Energy deposited in second H2	??	kW

5.5 Match solenoid to super FOFO lattice

A match is required between the approximately uniform 1.25 T solenoid fields in the phase rotation sections, and the alternating field 'super FOFO' lattices used in the bunching and cooling sections that follow. This match should be chromatically matched, but since the

momentum spread is relatively small ($\approx$ 4 % rms), the chromatic correction is less critical here than, for instance, in the field reversal.

The Tb. 13 gives coil dimensions and current densities for the match. Fig. 10 shows these coils, their fields, and the β's for three different momenta.

Table 13: Coil dimensions and current densities of matching solenoid to SUPER FOFO lattice

len1	dl	rad	dr		I/A
m	m	m	m		A/mm^2
0.000	1.375	0.300	0.100	2	-9.99
1.375	1.375	0.300	0.100	2	-9.99
2.750	1.375	0.300	0.100	2	-9.99
4.125	1.375	0.300	0.100	2	-9.99
5.500	1.375	0.300	0.100	2	-9.99
6.875	1.375	0.300	0.100	2	-9.99
8.250	0.330	0.300	0.110	2	-15.57
8.949	0.187	0.330	0.330	6	-33.40
9.466	0.187	0.330	0.330	6	35.19
10.511	0.330	0.770	0.110	2	66.12
11.665	0.187	0.330	0.330	6	43.75
12.182	0.187	0.330	0.330	6	-43.75
13.227	0.330	0.770	0.110	2	-67.40
14.415	0.187	0.330	0.330	6	-43.75
14.932	0.187	0.330	0.330	6	43.75
15.977	0.330	0.770	0.110	2	66.12
17.165	0.187	0.330	0.330	6	43.75

5.6 Buncher

The bunching is done in the same lattice as used for the first cooling stage (1,1), which is described in section 5.7. A total of 20 cells are used, giving it a length of $20 \times 2.75 = 55$ m.

The buncher consists of three stages:

1. low field 200 MHz rf with 400 MHz harmonic, followed by a long drift (27.5 m)
2. medium field 200 MHz rf with 400 MHz harmonic, followed by a shorter drift (7.75 m)
3. higher field 200 MHz rf followed by a short drift (5.5 m)

RF The locations and lengths of the RF components are listed in table 14.
The RF window radii and thicknesses are given in Tb. 15.
Buncher RF and windows new table

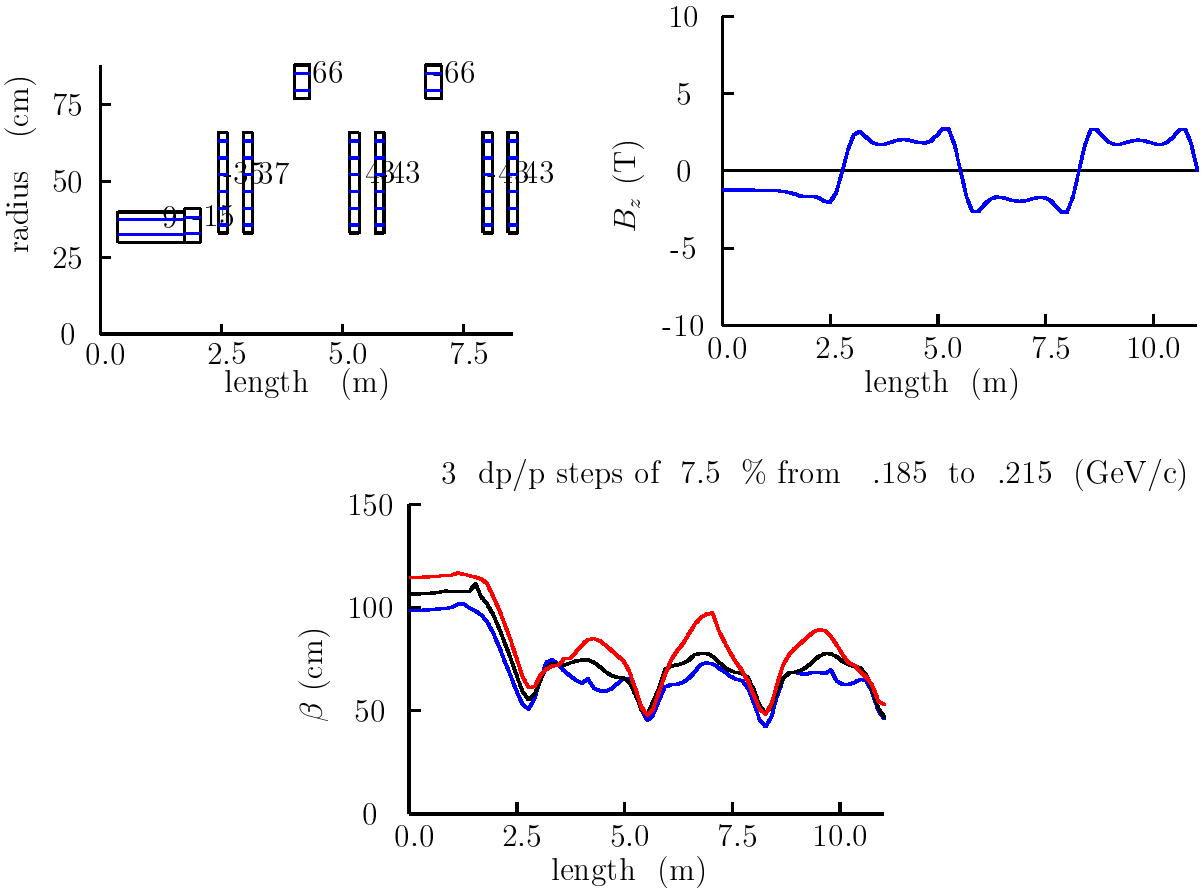

Figure 10: Top left: Coil arrangement for the matching section between the constant 1.25 T solenoid field and the first cell of the SUPER FOFO lattice; top right: Longitudinal field on axis; bottom: β function for momentum between 0.185 to 0.215 GeV/c.

type	sec	freq MHz	length m	grad MV/m	phase deg	thick μm	rad cm
buncher							
end	b1	402.5	.186	-6.4	0	75	18
end	b2	402.5	.186	-6	0	75	18
end	b1	201.25	.3728	6.4	0	103	21
end	b1	201.25	.3728	6.4	0	120	14
end	b2	201.25	.3748	6	0	100	21
end	b2	201.25	.3748	6	0	105	14
end	b3	201.25	.3748	8	12	180	21
end	b3	201.25	.3748	8	12	187	14

Table 14: Buncher: location and length of rf componentsold table

	len m	freq MHz	grad Mv/m
harmonic rf	.186	402.5	6.4
space	.443		
rf	4 × .373	201.25	6.4
space	.443		
harmonic rf	.186	402.5	6.4
drift 1	10 × 2.75		
harmonic rf	.186	402.5	6
space	.443		
rf	4 × .373	201.25	6
space	.443		
harmonic rf	2 × .186	402.5	6
space	.443		
rf	4 × .373	201.25	6
space	.443		
harmonic rf	.186	402.5	6
drift 2	3 × 2.75		
space	.629		
rf	4 × .373	201.25	8
space	.629		
space	.629		
rf	4 × .373	201.25	8
space	.629		
drift 3	2 × 2.75		

5.7 Cooling Lattices

Introduction The cooling is done in six sections with steadily decreasing β's. This is done to maximize the cooling rate. Too small a β at a given emittance results in too large divergence angles and particle loss. Too large a β gives small divergence angles and a greater relative emittance growth from Coulomb scattering. The best β scales down with the emittance and is always such as to give a certain constant rms divergence angle ($\sigma_{x'} = \sigma_{y'} \approx 0.1$).

The six sections are made from two different physical lattices [(1) and (2)], with three different current setting in each: 1,1 1,2 1,3 in the first lattice, and 2,1 2,2 2,3, in the second. The final cooling section (2,3) is further broken into 2 parts (2,3a) and (2,3b) that differ only in their window sizes and thicknesses.

The lengths of the sections are shown in Tb. 16

The lattices used have been named "Super FOFO"[?]. The "FOFO" refers to the basic

Table 15: rf window dimensions ***Needs correcting

	rad m	thickness μm
windows at ends of each 400 MHz cavity	.2	100
windows at end of each set of 4 200 MHz cavities	.21	125
windows between the 4 400 MHz cavities	.25	250

Table 16: Length of the ionization cooling lattices

	length m	total length m
cool 1,1	$4 \times 2.75 = 11$	11
match 1,1-2	$2 \times 2.75 = 5.5$	16.5
cool 1,2	$4 \times 2.75 = 11$	27.5
match 1,2-3	$2 \times 2.75 = 5.5$	33
cool 1,3	$4 \times 2.75 = 11$	44
match 1,3-2,1	4.4	48.4
cool 2,1	$12 \times 1.65 = 19.8$	68.2
match 2,1-2	$2 \times 1.65 = 3.3$	71.5
cool 2,2	$8 \times 1.65 = 13.2$	84.7
match 2,2-3	$2 \times 1.65 = 3.3$	88
cool 2,3	$12 \times 1.65 = 19.8$	107.8

sequence of alternating solenoids, that both focus (FOcus-FOcus) the beam and generate β and beam size, minima between the solenoids. The "Super" part, proposed by A. Sessler, is the replacement of the simple alternating solenoids with alternating, but more complex, solenoid systems. In this case the systems consist of strong short "focusing" solenoids at either end, and a weaker "coupling" fields between them. An example of the fields (for the last part) is given in Fig. 11 Figure 12 shows the beta functions, as a function of momentum, for the six cases discussed above.

In all cases the β functions are seen to have sharp drops above and below the required momentum acceptance. These are due to the approach to two resonances. At the lower momentum it corresponds to a 2 π phase advance per cell, and at the higher momentum to 1 π phase advance. With any given lattice length, the central beta and its location can be controlled by adjusting just two charachters of the focusing fields. The details of the fields are relatively unimportant, just these two characteristics:

- the strength of the opposed "focusing" fields near the lattice ends (the higher the fields, the higher the momentums focused)
- the general magnitude of the field in the central part of the lattice

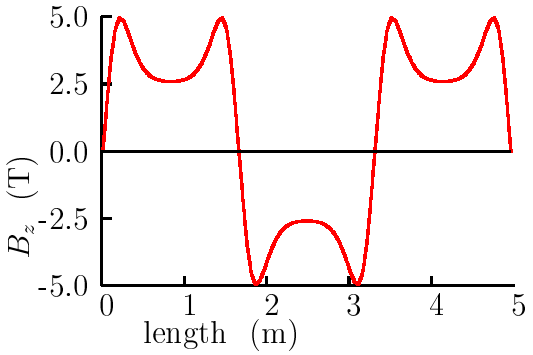

Figure 11: B_z on axis for the last cooling cell

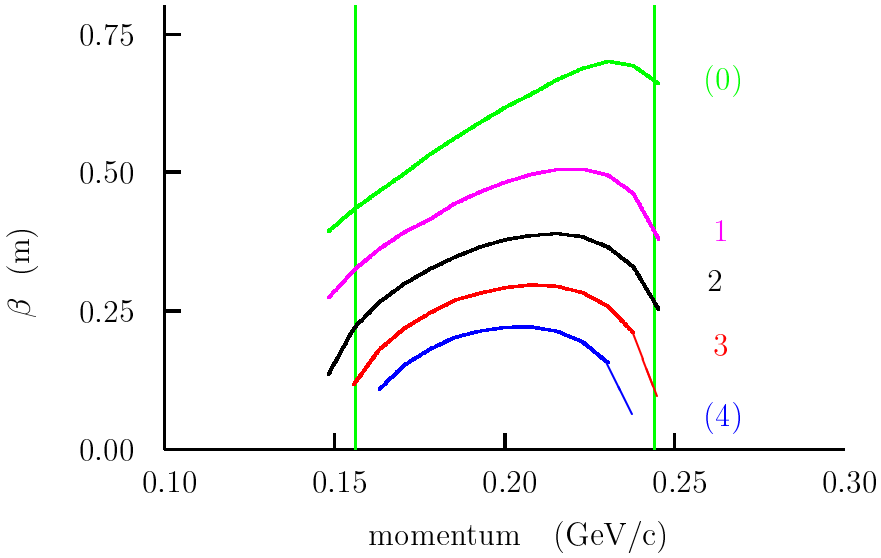

Figure 12: β function as a function of momentum for the 6 lattices discussed in the text

(a higher "coupling" field reduces the end betas, but increases the momentum acceptance)

By adjusting these two characteristics, we can keep the betas symmetric about the required mean momentum, and independently reduce the central beta value. But as we decrease the coupling fields, the momentum acceptance shrinks and, at some point, becomes unacceptably small. At this point we are forced to use a shorter lattice which, though it will require higher

fields, allows the betas to be further reduced while again achieving adequate momentum acceptance and keeping the betas symmetric.

In the chosen lattice, the two characteristics are controlled by the use of a separate "coupling" coil outside the RF, and power it independently of the "focusing" coils at the ends. This arrangement has the big advantage that the two parameters are just the two currents, and the betas can be varied, and the symmetry maintained, by adjusting these currents without changing the physical design. This done here, first with a 2.75 m long lattice, and then with a 1.65 m one. Three different sets of currents have been specified for each of the lattices, giving a total of six different central β's. If desired, the number of different currents could be further increased to make the change of parameters even more adiabatic, but this will not change the physical designs.

Specific coil dimensions, current densities and fields they generate are given below, but it should be understood that the exact shape of the fields is not important provided that the approximate locations and magnitudes of the end fields, and the approximate magnitude of the central fields are achieved.

The axial field along the full cooling channel are shown in Fig. 13. The different field and periodicities in the 6 regions can be clearly seen. The dimensions and currents of the coils are given in tables 17 andf 18.

Table 17: Geometric properties and current densities of solenoids for a 2.75 m long cell

len1	dl	rad	dr	j(1,1)	j(1,2)	j(1,3)
m	m	m	m		A/mm^2	
0.175	0.167	0.330	0.175	75.20	84.17	91.46
1.210	0.330	0.770	0.080	98.25	92.42	84.75
2.408	0.167	0.330	0.175	75.20	84.17	91.46

Table 18: Geometric properties and current densities of solenoids for a 1.65 m long cell

len1	dl	rad	dr	j(2,1)	j(2,2)	j(2,3)
m	m	m	m		A/mm^2	
0.066	0.145	0.198	0.330	68.87	75.13	83.48
0.627	0.396	0.792	0.099	95.65	87.00	76.52
1.439	0.145	0.198	0.330	68.87	75.13	83.48

5.8 Matching

Between Sections With Same Cell Length In all cases a matching section is inserted consisting of two cells: the first as in previous cells, the second as following cells, except that the currents in the central pair of focus coils are set to an average of the currents in the previous and following focus coils.

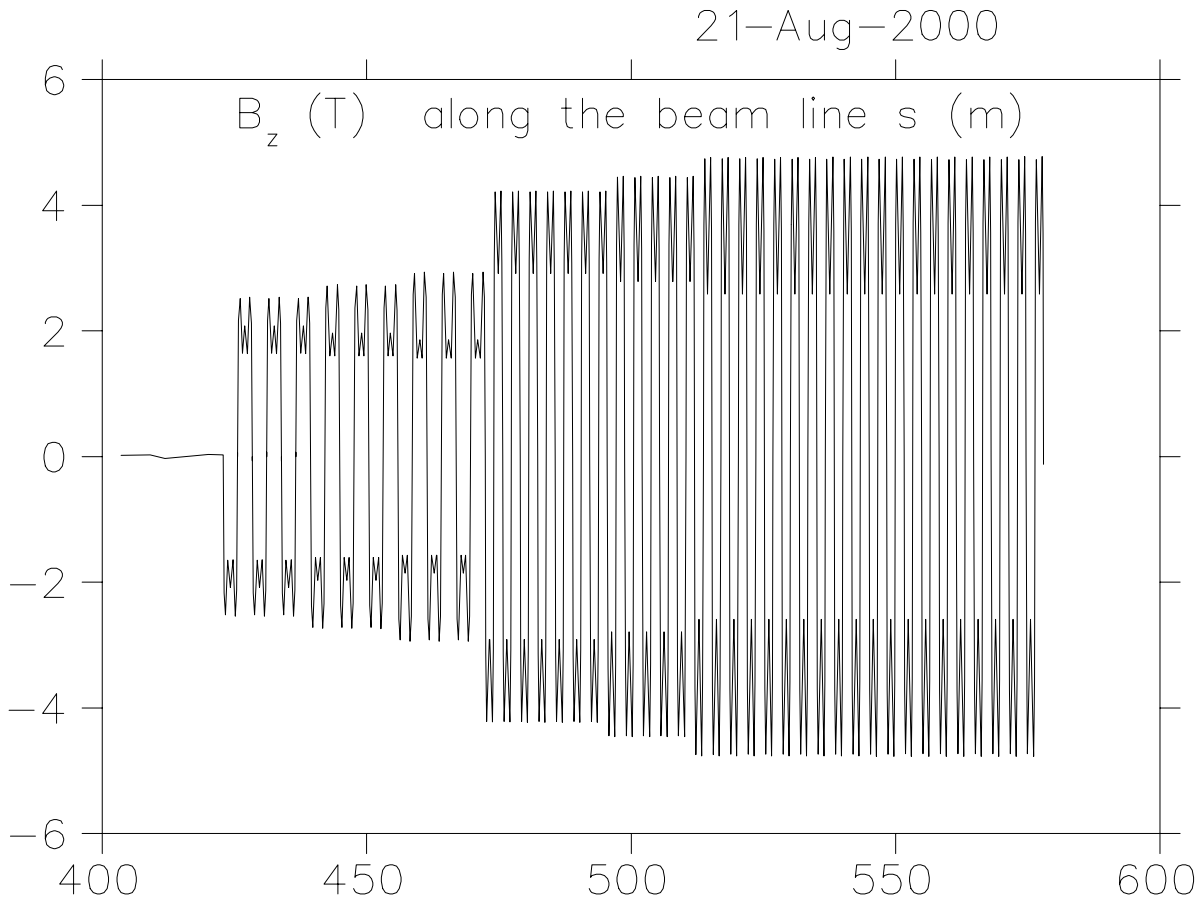

Figure 13: The axial field along the full cooling channel

For instance, the parameters for the match from 1,1 to 1,2 are given in Tb. 19.

The parameters of the matching between cells of different lengths (1,3 to 2,1) are given in Tb. 20. The coils are shown in Fig. 14, and the axial fields and beta functions for different momenta are shown in Figs. 15 and 16.

5.9 Cooling absorbers and RF

The hydrogen absorbers and rf within the three 2.75 m (or 1.65 m) lattices are all the same except for their apertures (which are given in the next section). The parameters for the two lattices and the match between them are given in Tbs. 21, 23, and 22. Note that there is no hydrogen in the center of the match and that the phases are adjusted to correct for the resulting lack of energy loss.

Table 19: Matching solenoid between sections with the same length

len1 m	gap m	dl m	rad m	dr m	I/A A/mm^2
last 1,1					
0.175	0.175	0.167	0.330	0.175	75.20
1.210	0.868	0.330	0.770	0.080	98.25
2.408	0.868	0.167	0.330	0.175	75.20
match					
2.925	0.175	0.167	0.330	0.175	-75.20
3.960	0.868	0.330	0.770	0.080	-98.25
5.158	0.868	0.167	0.330	0.175	-80.07
5.675	0.175	0.167	0.330	0.175	80.07
6.710	0.868	0.330	0.770	0.080	92.42
7.908	0.868	0.167	0.330	0.175	84.17
first 1,2					
8.425	0.175	0.167	0.330	0.175	-84.17
9.460	0.868	0.330	0.770	0.080	-92.42
10.658	0.868	0.167	0.330	0.175	-84.17

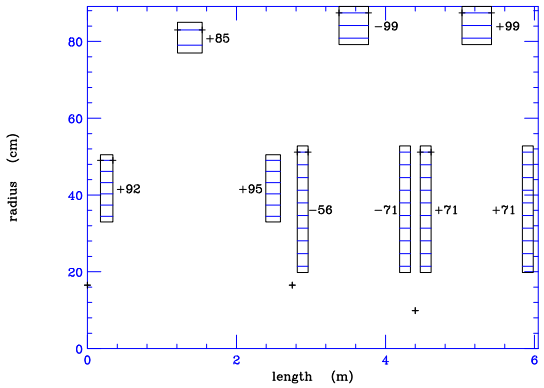

Figure 14: Matching (1,3) to (2,1): Coils positions and Current densities

5.10 RF Windows in Stepped Be Foil

The rf apertures are given in Tb. 25.

An alternative to the edge cooled Be foils, using a grid of gas cooled Al pipes is considered in appendix ??.

5.11 Acceleration

The requirements for the acceleration system are:

The number of muons specified correspond to a 1.5 MW driver and 0.2 μ's/p.

Table 20: Matching solenoid between sections with diferent lengths

len1 m	gap m	dl m	rad m	dr m	I/A A/mm^2	n I A	n I l A m
last 1,3							
2.925	0.175	0.167	0.330	0.175	91.46	2.70	7.08
3.960	0.868	0.330	0.770	0.080	84.75	2.26	11.50
5.158	0.868	0.167	0.330	0.175	91.46	2.70	7.08
match							
5.675	0.175	0.167	0.330	0.175	-91.46	2.70	7.08
6.710	0.868	0.330	0.770	0.080	-84.75	2.26	11.50
7.893	0.853	0.198	0.330	0.175	-95.24	3.30	8.66
8.316	0.066	0.145	0.198	0.330	56.39	2.70	6.16
8.877	0.416	0.396	0.792	0.099	95.65	3.75	19.83
9.689	0.416	0.145	0.198	0.330	68.87	3.30	7.53
first 2,1							
9.966	0.066	0.145	0.198	0.330	-68.87	3.30	7.53
10.527	0.416	0.396	0.792	0.099	-95.65	3.75	19.83
11.339	0.416	0.145	0.198	0.330	-68.87	3.30	7.53

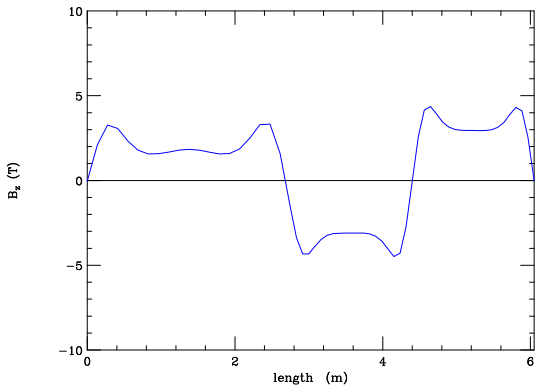

Figure 15: Matching (1,3) to (2,1):B_z on axis vs z

5.12 Storage Ring

Alternative to Soudan

target material & proton energy For comparison with Feasibility Study 1, we have run the program with a carbon target (80 cm long, at 50 mrad) and 16 GeV proton energy. These are given below together with the study 1 values.

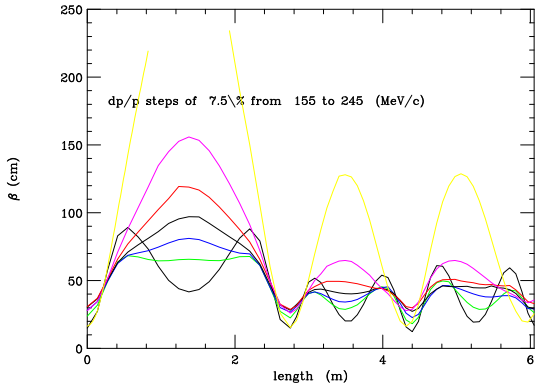

Figure 16: Matching (1,3) to (2,1):β function vs z for different momentum in steps of $\frac{dp}{p}$ = 7.5 % from 155. to 245. MeV/c

Table 21: 2.75 m lattices: Cooling rf

	dl cm	gradient MV/m	phase deg
Hydrogen	35/2		
Space	26.5		
RF	4 × 46.6	15.48	40
Space	26.5		
Hydrogen	35/2		

	p energy GeV	rms bunch length ns	μ/p 15 mm	μ/p 9.75
Mercury	24	3	0.20	.164
Carbon	16	3	.069	.057
Carbon (Study 1)	16	3		.018

So the gain over Study 1 from the capture and cooling design improvements is 3.2 ×; the gain from the use of the mercury target is 1.9 ×; and from the use of a larger accelerator acceptance is 1.2 ×; for a total gain of 7.4 ×. It should be noted that other authors have also reported cooling schemes with efficiencies substantially greater than those in the Feasibility Study 1. It is believed, never the less, that the scheme proposed here has significant advantages.

6 REFERENCES

[1] N. Holtkamp, D. Finley,Editors, A Feasibility Study of a Neutrino Factory Based on a Muon Storage Ring,Aug., 2000

Table 22: Match from (1,3) to (2,1): Cooling rf

	dl cm	gradient MV/m	phase deg
Hydrogen	35/2		
Space	26.4		
RF	4 × 46.6	15.48	18.8
Space	70.5		
RF	2 × 55.9	16.72	18.8
Space	15.9		
Hydrogen	21/2		

Table 23: 1.65 m lattices: Cooling rf

	dl cm	gradient MV/m	phase deg
Hydrogen	21/2		
Space	16		
RF	2 × 55.9	16.72	40
Space	16		
Hydrogen	21/2		

http://www.fnal.gov/projects/muon_collider/nu-factory/fermi_study_after_april1st/

.

Table 24: Hydrogen Windows

sec	H2		
	t	r	mat
	μm	cm	
1,1-3	360	18	Al
2,1-3	220	11	Al

Table 25: rf Windows in Stepped Be Foil *** needs updating

Sec	ends					center				
	t2	t1	r1	r2	mat	t2	t1	r1	r2	mat
	μm	μm	cm	cm		μm	μm	cm	cm	
1,1-3	400	200	12	18	Be	1400	700	14	21	Be
Match 1,3 to 2,1	400	200	12	18	Be	1400	700	14	21	Be
2,1-3	200	100	10	15	Be	760	380	12	18	Be

Table 26: Requirements acceleration system

initial momentum	210	MeV/c
final energy	20	GeV
Transverse acceptance	15	mm rad
Longitudinal acceptance	150	mm
bunch spacing	201.25	MHz
number of bunches	67	
total muons per bunch train	3	10^{13}

Table 27: Storage Ring to WIPP

To Carlsbad	2903	km
Dip angle	13.1	deg
Dip angle	.229	rad
Bearing	267.45	deg
Tunnel diam	10	ft
Cover	20	ft
Burm angle	27	deg
Arc Rad	16.9	m
Water table	45	ft
Decay len / circ	35	%

Table 28: Storage ring: layout constraints

decay/circ %	circ. m	decay m	len m	dh m	hill m	vol yrd^3
35	332	116	148	34	30	225k

Table 29: Storage ring to Soudan

To Soudan	1713	km
Dip angle	7.73	deg
Dip angle	.134	rad
Bearing	303.33	deg
Decay len / circ	40	%

Table 30: Storage ring: layout constraints

decay/circ %	circ. m	decay m	len m	dh m	hill m	vol yrd^3
40	550	220	252	34	30	250k